

## CHAPTER 183

### SEDIMENT TRANSPORT UNDER (NON)-LINEAR WAVES AND CURRENTS

Jan S. Ribberink<sup>1)</sup>, Irene Katopodi<sup>2)</sup>, Khaled A.H. Ramadan<sup>3)</sup>,  
Ria Koelewijn<sup>4)</sup> and Sandro Longo<sup>5)</sup>

#### Abstract

Two series of experiments were carried out in the Large Oscillating Water Tunnel of Delft Hydraulics, which was recently extended with a recirculation flow system. Combined wave-current boundary layer flows were studied with a mobile sand bed in the sheet flow regime. Detailed intra-wave concentration and velocity measurements were carried out and revealed a three-layer system, i.e. a pick-up layer, a sheet flow layer and a suspension layer. In the suspension layer time-lag effects of the sediment concentration led to sediment fluxes in upstream direction. The suspended sediment was more confined to the near-bed region than according to diffusion theories, most likely due to turbulence damping. The horizontal time-dependent and net sediment fluxes were concentrated in the sheet flow and pick-up layer. Measured net sediment transport rates could be described as a linear relation with the third-order velocity moment  $\langle U^3 \rangle$  near the bed.

- 
- 1) Senior research officer, Delft Hydraulics, P.O. Box 152, 8300 AD Emmeloord, The Netherlands and: Delft University of Technology (Netherlands Centre of Coastal Research)
  - 2) Scientific officer, Democritus University of Thrace, Department of Civil Engineering, 67100 Xanthi, Greece
  - 3) Research officer, Hydraulics & Sediment Research Institute, P.O. Box 13621, Delta Barrage, Egypt
  - 4) M.Sc. student, Delft University of Technology, Fac. of Civ. Eng., Hydr. Eng. Section, P.O. 5048, 2600 GA Delft, The Netherlands
  - 5) Researcher, University of Florence, Department of Civil Engineering, via S.Marta 3, 50139 Florence, Italy

## Introduction

The understanding of the physical processes near the sea bed in combined wave-current flows plays an essential role in the description of the sediment transport in the coastal zone. A general lack of basic knowledge on the interaction between waves, currents, sediments and the sea bed in the combined wave-current boundary layer exists. The validity of various mathematical models can hardly be assessed due to the low number of measurements available, especially at prototype scale (Horikawa, 1988). The present study is focused on the boundary layer processes in the case of high bed-shear stress conditions (Shields parameter  $> 0.6$ ). In this regime the sea bed is plane with sheet flow and suspension as the dominating transport modes. A research programme is concentrated around the Large Oscillating Water Tunnel of Delft Hydraulics in which the wave-induced near bed oscillatory flow and sediment transport phenomena can be simulated in the scale of nature (1:1). The present research is a follow-up of earlier work by Ribberink and Al-Salem (1994) and Al-Salem (1993) whom collected a large series of data on the sediment dynamics in mainly asymmetric oscillatory flow conditions. They verified and developed several mathematical models for the description of the observed phenomena. In 1992 the tunnel was extended with a recirculation flow system (see Figure 1) which enabled the superposition of net currents to the oscillatory flow. During a first experimental programme the behaviour of the tunnel flow and the various bedform regimes were investigated in regular wave-current conditions (Ramadan, 1993).

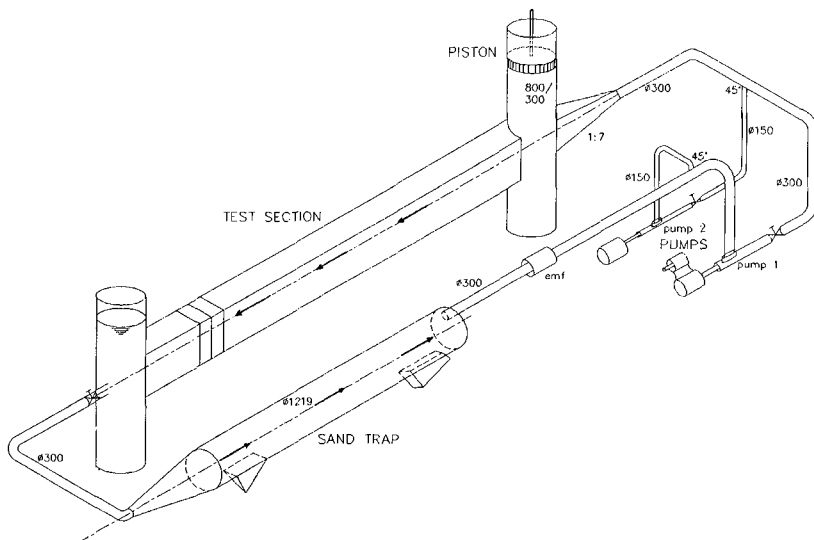


Figure 1 The Large Oscillating Water Tunnel with its recirculation system

In the present paper the main results of two experiment series (series C and E) are presented. Series C was focused on the influence a net current superimposed on asymmetric (second-order Stokes) waves on time-averaged quantities such as the suspended load and the net sediment transport rate.

During series E detailed time-dependent (intra-wave) measurements were carried out in the suspension layer and the sheet flow layer in a number of sinusoidal wave/net current combinations.

The main objectives of the experiments were: i) to increase the understanding of the wave-current boundary layer processes in the case of mobile sandy beds, and ii) to obtain a number of datasets to be used for the development of sediment transport models.

For the complete experimental results, reference is made to the original data reports, i.e. Ramadan (1993), Ribberink (1994) and Katopodi et al (1994).

### Experimental set-up and programme

The Large Oscillating Water Tunnel (LOWT) has the shape of a vertical U-tube with a long rectangular horizontal section and two cylindrical risers on either end. The desired oscillatory water motion inside the test section is imposed by a steel piston in one of the risers. The other riser is open to the atmosphere. The test section is 14 m long, 1.1 m high and 0.3 m wide. A 0.3 m thick sand bed can be brought into the test section, leaving 0.8 m free for the oscillatory flow above the bed. The range of the oscillatory velocity amplitudes is 0.2-1.8 m/s and the range of periods is 4-15 s. The LOWT, extended with a recirculation flow system for the generation of a steady current, is shown in Figure 1. The maximum capacity of the two pumps is 100 l/s and 20 l/s. The maximum superimposed mean current velocity in the test section is 0.5 m/s. The two risers are used as sand traps, moreover the recirculation system is provided with a 12 m long pipe sand trap.

As a follow-up of previous research with asymmetric (second-order Stokes) waves (Ribberink and Al-Salem, 1994), a series of experiments was conducted (series C) with asymmetric waves combined with following and opposing currents (following current = a positive current in the direction of the crest half wave cycle motion). In total 10 conditions were investigated. Series C was mainly aimed at the measurement of time-averaged concentrations and sediment transport rates. Each condition was repeated 3-5 times. Each test started with a flat horizontal sand bed. Table 1 gives the main flow characteristics of series C, i.e. the pump discharge  $Q$ , the mean current velocity in the test section  $\langle U \rangle$ , the root mean square velocity of the oscillatory flow part  $\tilde{U}_{rms}$  and the wave period  $T$ . Sand was used with characteristics  $D_{10} = 0.15$  mm,  $D_{50} = 0.21$  mm and  $D_{90} = 0.32$  mm.

Detailed time-dependent measurements were carried out during series E for four sinusoidal wave/net current conditions (see Table 2). From E1 to E4 the oscillatory velocity amplitude  $\hat{U}$  decreases but the net current velocity increases in such a way that the third-order velocity moment  $\langle U^3 \rangle$  of the horizontal oscillatory flow (above

the wave boundary layer) is approximately constant. This choice was based on the linear relation between the net transport rate and  $\langle U^3 \rangle$  as found by Al-Salem (1993) for only (asymmetric) waves. During 5 series of experiments different measuring techniques were used and 115 tests (tunnel runs) were carried out using the same sand as for series C.

Exp.	Net current		Oscillatory flow	
	Q (m <sup>3</sup> /s)	$\langle U \rangle$ (m/s)	$\hat{U}_{rms}$	T (s)
C1	0	0	0.56	6.5
C2	0.012	0.05	0.56	6.5
C3	0.072	0.3	0.55	6.5
C4	0.036	0.15	0.56	6.5
C5	0.096	0.4	0.55	6.5
C9	0	0	0.56	6.5
C10	0.096	0.4	0.8	6.5
C11	0	0	0.8	6.5
C12	0.024	0.1	0.8	6.5
C13	0.096	0.4	0.8	6.5

Table 1 Experimental conditions series C (sheet flow)

Exp.	Net current		Oscillatory flow	
	Q (m <sup>3</sup> /s)	$\langle U \rangle$ (m/s)	$\hat{U}$ (m/s)	T (s)
E1	0.036	0.15	1.6	7.2
E2	0.048	0.20	1.35	7.2
E3	0.072	0.30	1.10	7.2
E4	0.096	0.40	0.9	7.2

Table 2 Experimental conditions series E (sheet flow)

Suspended sediment concentrations in the range of 0.1 - 50 g/l were measured with a transverse suction technique for time-averaged values (series C, E) and an optical infra-red light extinction technique OPCON for time-dependent values (series E).

The large (time-dependent) concentrations in the sheet flow layer ( 100-1600 g/l) were measured with an electro-resistance technique CCM (series E).

Time-dependent velocities were measured with a 2 component forward-scatter laser-doppler flow meter LDFM for mainly clear water (series C, E), an electro-magnetic flow meter EMF in the suspension layer (series C,E) and a high-speed video technique HSV for grain velocities in the sheet flow layer (series E). Net sediment transport rates were measured with a mass-conservation technique using sand trap volumes and measured bed-level changes. For more detailed information about the techniques, reference is made to Katopodi et al (1994).

Suspended sediment

During the 10 series C and 4 series E conditions totally 81 time-averaged concentration profiles were measured with the transverse suction technique in the layer between 1-1.5 cm and 25 cm above the bed.

In Figure 2 all suspended concentration profiles of series E are plotted on a log-log x-y scale. The straight best-fit lines imply a vertical distribution according to the following power-law:

$$\frac{\langle C(z) \rangle}{C_a} = \left( \frac{z_a}{z} \right)^\alpha$$

where  $C_a$  is a reference concentration at the level  $z_a$  and the power  $\alpha$  is a concentration decay parameter.

Despite the different combinations of waves and currents during series E, the best-fit lines are almost parallel, indicating that the power  $\alpha$  is almost constant ( $1.9 < \alpha < 2.4$ ).

Also for the series C experiments the power-law distribution (1) fitted well with the measurements. The concentration decay parameter  $\alpha$  varied between  $1.6 < \alpha < 2.3$ .

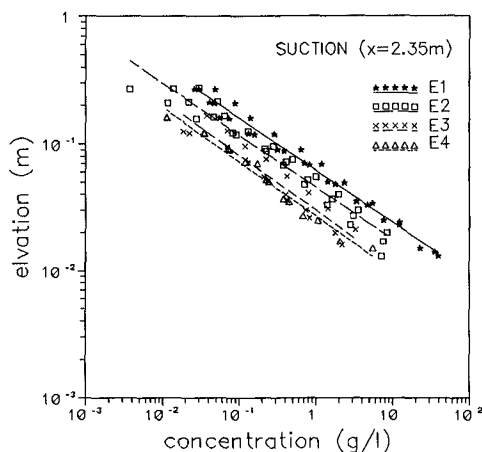


Figure 2 Time-averaged concentration profiles of suspended sediment, series E

Ribberink and Al-Salem (1994) found the same power-law form for a large number of waves-only cases in the sheet flow regime (same sand). The power  $\alpha$  was almost constant ( $\alpha \approx 2.1$ ) in a wide velocity range ( $U_{rms} = 0.3-1.2$  m/s). Figure 3 shows power  $\alpha$  as a function of the maximum Shields number  $\theta'_{max}$  (maximum value during the wave cycle) for the 'waves alone' measurements and the new 'waves + currents' measurements.

$\theta'_{max}$  is computed on the basis of the maximum bed-shear stress during the wave cycle according to:

$$\theta'_{max} = \frac{\tau'_{b_{max}}}{(\rho_s - \rho) g D_{50}}$$

Herein  $\tau'_{b_{max}} = 0.5 \rho f_{cw} (\langle U \rangle + \hat{U})^2$  with the combined wave-current friction factor according to the theory of Jonsson (1966) using  $k_s = D_{50}$  as bed roughness height. The measured values of  $\langle U \rangle$  at  $z = 10$  cm above the bed are used as input for the formulation.

Figure 3 shows that all measured values of alpha (for waves alone and waves + currents) scatter around  $\alpha = 2$ , showing no relation with the Shields number.

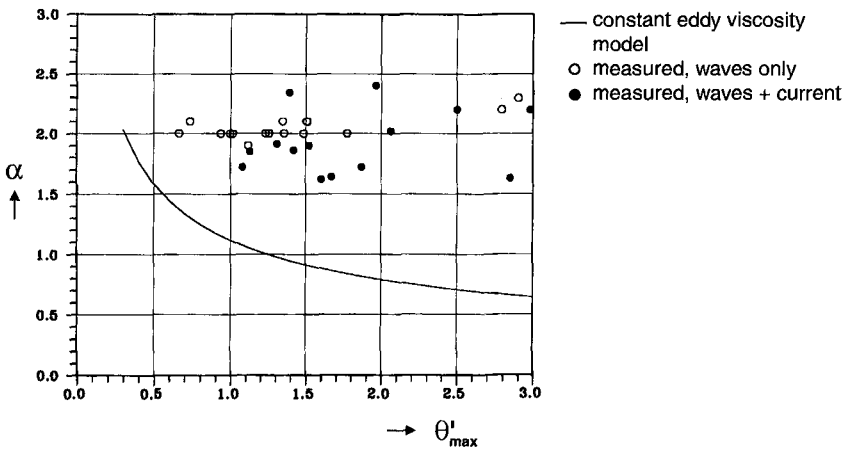


Figure 3 Concentration decay parameter  $\alpha$  vs. maximum Shields number

In the case of a time-invariant sediment mixing or diffusion coefficient increasing linearly with distance above the bed, diffusion models for suspended sediment generate a similar power-law distribution for the time-averaged concentration (see Ribberink and Al-Salem, 1994). However, the models generally lead to decreasing values of  $\alpha$  (= Rouse number) for increasing Shields numbers. This is due to an increasing turbulent or sediment mixing coefficient with increasing bed-shear stress. The full line in Figure 3 represents the theoretical solution of the Rouse number. It is shown that the measured concentration decay is always greater than the theoretical decay and shows no relation with the Shields number.

Apparently, the suspended sediment is more confined to the near-bed region than the theory predicts. Moreover, the result indicates the increasing importance of turbulence damping above the mobile bed (sheet flow layer) for increasing Shields numbers.

The measured time-dependent behaviour of the suspended sediment concentrations during experiment E1 is shown in Figure 4. In the lower part ensemble-averaged concentrations measured with OPCON are shown during one wave cycle at three elevations near the bed. The upper part shows the time-dependent horizontal velocity (at  $z = 20$  cm) as well as the vertical position of the piston driving the oscillatory flow.

It can be observed that the concentration exhibits two peaks that roughly coincide with the maximum downstream and upstream velocities. Due to the asymmetry of the flow (downstream velocity amplitude  $>$  upstream velocity amplitude) the two peaks are not of equal magnitude. Two other generally smaller concentration peaks occur near the moments of flow reversal. Similar peaks were observed by Al-Salem (1993) for waves only. A possible explanation for their existence may be found in turbulence generation due to shear instabilities in the bottom boundary layer (see Foster et al, 1994).

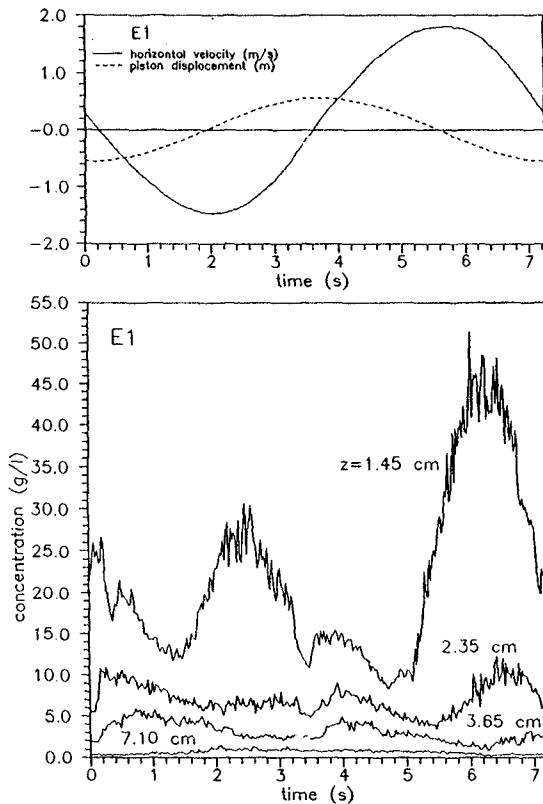


Figure 4 Time-dependent suspended sediment concentrations, E1

With increasing distance above the bed the concentration decays rapidly and the concentration maxima occur at a later moment (time lag effect). At higher elevations

the maximum concentrations occur even after the next flow reversal, indicating history effects from a previous half wave cycle.

From E1 to E4 the flow asymmetry increases due to an increasing net current velocity/oscillatory velocity ratio (see Table 2). Simultaneously, the concentration measurements show an increasing history effect of the 'downstream' half cycle during the 'upstream' half cycle. Moreover, the concentration peaks at flow reversal become less dominant. For more detailed results, see Katapodi et al (1994a).

### Sheet flow

At lower elevations near the bed ( $z < 1$  cm) the sheet flow layer is entered with very large sediment concentrations (100-1600 g/l). Time-dependent concentration measurements were carried out with the CCM. The CCM was brought into the test section from below through the sand bed in order to minimize possible flow disturbance. The lower part of Figure 5 shows ensemble-averaged concentrations (E1) at various elevations around  $z = 0$ . The elevation  $z = 0$  is defined as the mean bed elevation before/after the experiment (without sediment motion). The upper part of Figure 5 shows the time-dependent velocity at  $z = 20$  cm.

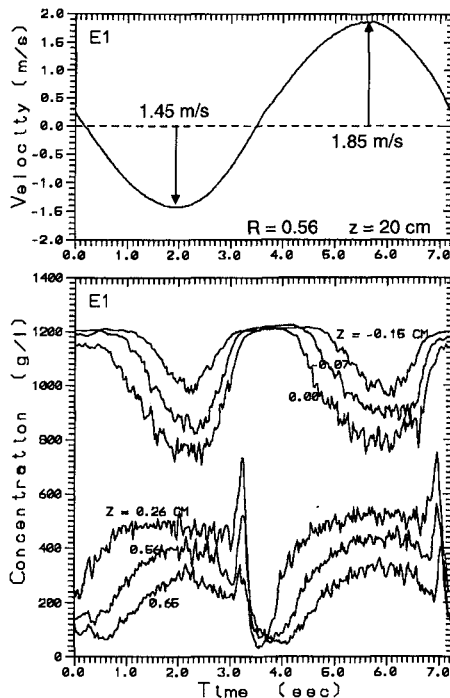


Figure 5 Time-dependent concentrations in the sheet flow layer, E1

Two layers with different behaviour can clearly be observed, i.e. a pick-up layer with minimum concentrations in phase with maximum velocities and a sheet flow layer with maximum concentrations in phase with maximum velocities. In the pick-up layer two phases occur during each wave cycle with no sediment motion and maximum sand concentration (settled sand, near  $U = 0$ ), which are both followed by a phase with lower concentrations due to the vertical pick-up of grains. In the sheet flow layer ( $z > 0$ ) the phase behaviour is opposite, reflecting the exchange of sand with the pick-up layer (see also Al-Salem, 1993). Near the moments of flow reversal large concentration peaks with a short duration occur, which are probably related with similar peaks as observed in the suspension layer somewhat later in time (see Figure 4). In general, all series E experiments show very small phase shifts between the concentration peaks at different elevations, indicating that time-lag effects are of minor importance in these near-bed layers.

The concentrations in the sheet flow layer do not show the asymmetry of the two half cycles as observed in the suspension layer of E1. However, for E2...E4 the increasing flow asymmetry effect becomes also visible in the sheet flow layer.

Figure 6 shows the complete time-averaged concentration profile on a log-linear x-y scale for all layers of E1 obtained from the CCM, OPCON and SUCTION measurements. The approximate positions of the suspension layer ( $C < 100$  g/l), the sheet flow layer ( $C > 100$  g/l) and the pick-up layer are indicated.

In the upward direction the concentration profile shows the transition from a convex shape (pick-up layer) to a concave shape (suspension layer), reflecting the presence of different physical mechanisms of the mixing process.

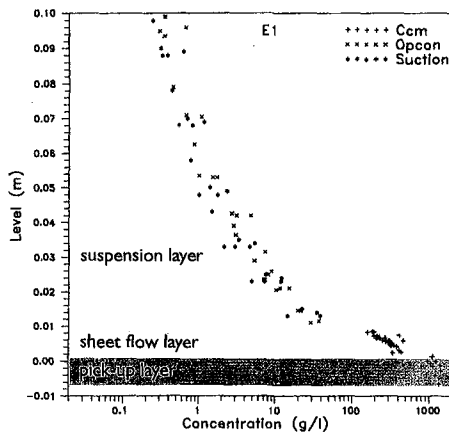


Figure 6 Time-averaged concentration profile of E1, a three-layer system

A high-speed video camera (500 frames/s) was focused through the glass side wall 2 cm inside the test section on a vertical image of 1.55 x 2.15 cm parallel to the oscillatory flow direction. A time counter on the video image was synchronized with

the piston motion. Two different particle tracking techniques were applied to measure the grain velocities at a number of phases of the cycle at several elevations above the bed.

Figure 7 shows measured horizontal grain velocity profiles of E1. Large velocity gradients occur especially in the sheet-flow and pick-up layer.

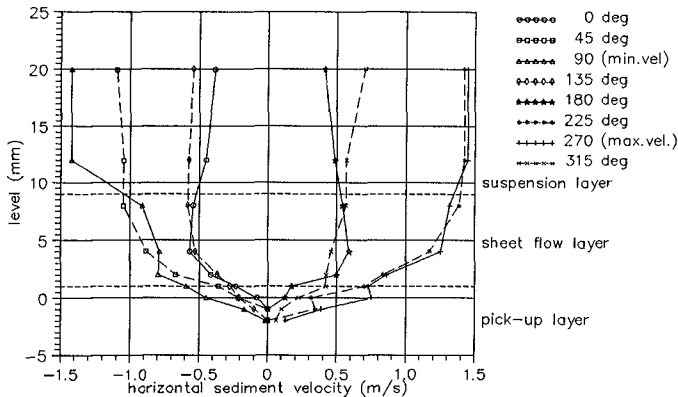


Figure 7 Horizontal grain velocity profiles of E1 (obtained with high-speed video)

### Sediment fluxes and net sediment transport rates

By multiplication of the horizontal velocities  $U(z,t)$  (LDFM, EMF) and concentrations  $C(z,t)$  (OPCON), time-dependent horizontal sediment fluxes  $\phi(z,t)$  were calculated in the suspension layer. The same was done in the sheet flow layer using the horizontal grain velocities (HSV) and the concentrations (CCM). The result of this analysis for experiment E1 is shown in Figure 8, using a log-linear x-y scale (with  $\phi = \pm 10^{-3}$  m/s as separation between negative and positive fluxes). The dimensionless volume concentration is used for the flux computation, and thus the sediment flux unit is m/s.

Maximum fluxes occur at the moments of maximum downstream and upstream velocity (above the wave boundary layer) in the sheet flow layer. Deeper into the sheet flow and pick-up layer the fluxes gradually reduce. A very strong reduction of the fluxes occurs in the suspension layer. The net horizontal sediment fluxes over the wave cycle were computed by time-averaging, making distinction between a current related and a wave related contribution, according to:

$$\langle \phi(z,t) \rangle = \langle U(z,t) \cdot C(z,t) \rangle = \phi_c + \phi_w$$

$$\phi_c = \langle U(z,t) \rangle \cdot \langle C(z,t) \rangle$$

$$\phi_w = \langle \tilde{U}(z,t) \cdot \tilde{C}(z,t) \rangle$$

Herein  $\tilde{U}$  and  $\tilde{C}$  represent the periodic parts of  $U$  and  $C$  after subtracting the wave-mean values  $\langle U \rangle$  and  $\langle C \rangle$  respectively. The distinction between  $\phi_c$  and  $\phi_w$  was only possible in the suspension layer where the mean velocity  $\langle U \rangle$  could be computed with a reasonable accuracy.

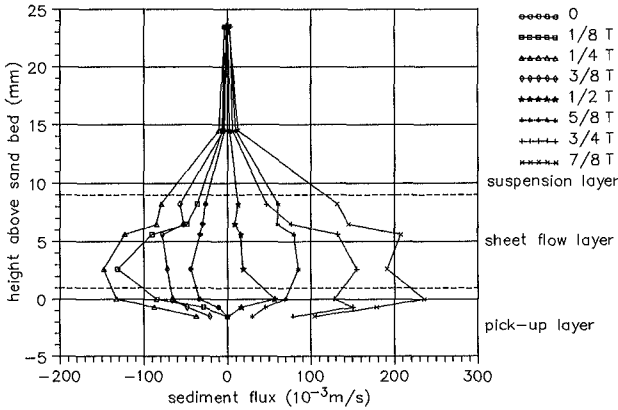


Figure 8 Time-dependent horizontal sediment flux profiles, E1

Figure 9 shows the computed net sediment flux profiles of the suspension layer of E1.

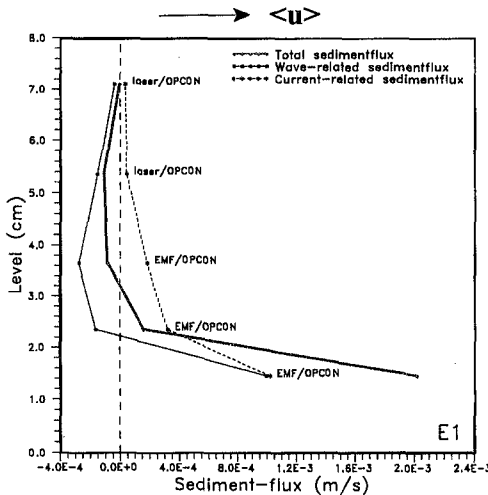


Figure 9 Net horizontal sediment flux profiles in the suspension layer, E1

It can be observed that due to time lags of  $\tilde{C}$  with respect to  $\tilde{U}$  (phase differences) a negative wave related flux is present at elevations  $z > 2$  cm. However, this negative contribution is almost compensated by the positive contribution of the current-related flux (the latter is positive by definition). Closer to the bed ( $z < 2$  cm) both contributions become positive and a relatively large positive total net flux results, showing a strong increase in the direction of the bed.

The complete total net horizontal flux profile for E1 is shown in Figure 10. In comparison with Figure 9 the scale of the horizontal axis had to be changed considerably (factor 10), due to the large magnitude of the net fluxes in the sheet flow and pick-up layer. The fluxes in the suspension layer can now hardly be recognized, indicating their minor importance for the total net sediment transport rate.

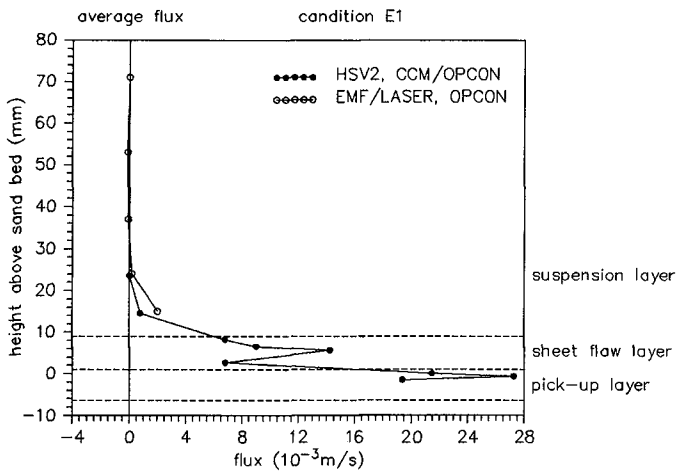


Figure 10 Total net horizontal sediment flux profile, E1

The fluxes in the sheet flow and pick-up layer show a considerable scatter, which is mainly caused by the low number of measured grain velocities per wave cycle in combination with a low accuracy of the grain velocity measurements. Vertical integration of the flux profile was carried out to estimate the total net sediment transport rate during E1. The obtained transport rate ( $120 \cdot 10^{-6} \text{ m}^2/\text{s}$ ) agreed reasonably well with the (relatively accurate) total net transport rate as obtained with the mass conservation technique ( $92.4 \cdot 10^{-6} \text{ m}^2/\text{s}$ ).

Also the experiments E2...E4 confirmed the result of experiment E1, namely that the net transport rate is mainly concentrated in the sheet flow and the pick-up layer. Even for E4 with the greatest net current the contribution of the suspension layer to the total net transport rate is minor. The previously mentioned relatively small

suspended sediment mixing above the mobile bed, most likely caused by turbulence damping effects of the sheet flow layer, is responsible for this phenomenon.

The results are only valid for the investigated conditions. It is expected that for finer sand, an increased current dominance (with respect to the waves) and in cases with rippled beds the importance of suspended sediment will strongly increase.

Al-Salem (1993) showed that in case of asymmetric 2<sup>nd</sup> order Stokes waves the net sediment transport is also concentrated in the sheet flow layer (same sand). Ribberink and Al-Salem (1994) showed that the net sediment transport can be described with a linear function of  $\langle U^3 \rangle$ , i.e. the third-order moment of the horizontal velocity above the wave boundary layer.

The measured net sediment transport rates of the series C and the series E experiments (totally 69 tunnel runs) were used to verify this relation in the case of combined waves and currents. The result is shown in Figure 11.

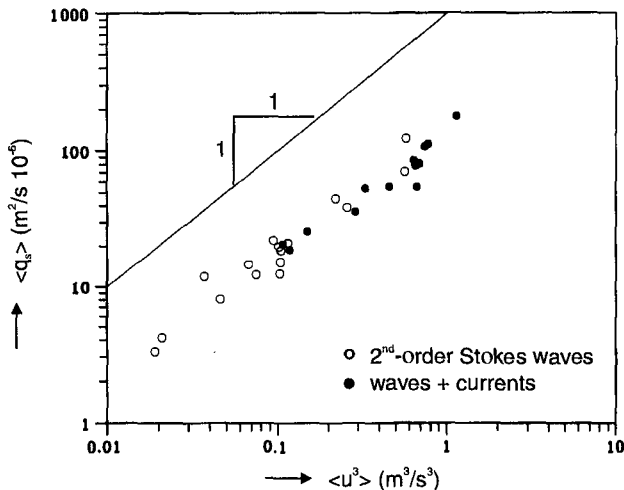


Figure 11 Measured net sediment transport rates vs. velocity moments  $\langle U^3 \rangle$

As the net current velocity is a function of the elevation above the bed and the velocity moment is computed on the basis of measured velocities, a choice was made for  $z = 10$  cm (series C) and  $z = 20$  cm (series E). Both elevations are above the wave boundary layer. The influence of the difference in the selected elevation (10 or 20 cm) on Figure 11 appeared to be minor.

The 'wave+current' cases in Figure 11 show approximately the same correlation between  $\langle q_s \rangle$  and  $\langle U^3 \rangle$  as the previous 'waves alone' cases.

The reasonable success of this relation (for this sand type and the selected experimental conditions) can be explained by the concentration of the sediment

transport near the bed (sheet flow layer) and the quasi-steady character of the transport process in this layer.

### Conclusions

Two experimental studies were conducted in the Large Oscillating Water Tunnel of Delft Hydraulics which was recently extended with a new recirculation system. Detailed time-dependent measurements were carried out in the combined wave current boundary layer in sheet flow conditions (series E) using a number of measuring techniques, among them a high-speed video technique for the measurement of grain velocities in the sheet flow layer. Series C concerned time-averaged measurements near the bottom. The datasets obtained can be used for the verification and development of boundary layer flow and transport models. In the present study a first analysis of the experimental results was presented.

The main conclusions are:

1. The time-dependent measurements of series E revealed a three layer transport system, viz. a pick-up layer, a sheet flow layer and a suspension layer with:
  - 4 concentration peaks per wave cycle in the sheet flow and suspension layer, (2 main peaks related to the maximum downstream and upstream velocities and 2 peaks near flow reversal),
  - increasing phase lags for increasing elevation in the suspension layer and almost no phase lags in the sheet flow and pick-up layer.
2. The time-averaged suspended sediment concentration profiles showed a similar negative power distribution as found during previous experiments with only waves. The concentration decay parameter  $\alpha$  appeared to be almost constant ( $\approx 2$ ) for all experiments (waves alone and waves + currents). The measured concentration decay near the bed was larger than the predicted decay of a theoretical diffusion model (with a time-invariant diffusion coefficient) and did not show the expected decrease for increasing Shields numbers. This is probably caused by turbulence damping effects above the mobile bed (sheet flow layer).
3. Using the time-dependent velocity and concentration measurements horizontal time-dependent and time-averaged sediment fluxes were computed and analyzed. The horizontal fluxes were concentrated in the sheet flow and pick-up layer near the bed. The contribution of the suspension layer to the total net flux appeared to be minor.
4. Due to the quasi-steady character of the transport process in the sheet flow and pick-up layer the measured net sediment transport rates of series C and series E showed a similar linear relation with  $\langle U^3 \rangle$  as obtained during previous experiments with asymmetric waves and no current.

### Acknowledgements

The series C experiments were carried out in the framework of the Coastal Genesis research programme in the Netherlands and were funded by the Ministry of Transport and Public Works (Directorate General Rijkswaterstaat).

The series E experiments were part of the European programme "Access to Large-scale Facilities and Installations" and were funded by the Commission of the European Communities, Directorate General for Science, Research and Development, contract no. GE1\*-CT91-0032 (HSMU). The research was executed by a European team with members, apart from the authors, also P. Ruol, C. Lodahl, A. Crosato and H. Wallace. The data analysis and reporting was partly done in the framework of the MAST G8, Coastal Morphodynamics research programme of the Commission of the European Communities, contract no. MaS2-CT92-0027. The assistance of M. Janssen with the computation of the sediment fluxes is greatly acknowledged.

### References

- Al-Salem, A.A. (1993). Sediment transport in oscillatory boundary layers under sheet-flow conditions, Ph. D. Thesis, Delft University of Technology.
- Horikawa, K. (ed) (1988). Nearshore dynamics and Coastal Processes, University of Tokyo Press, Tokyo, 522 pp.
- Jonsson, I.G. (1966). The friction factor for a current superimposed on waves, Basic Research-Progress Report No. 11, Technical University of Denmark, pp 1-12.
- Katopodi, I., J.S. Ribberink, P. Ruol, R. Koelewijn, C. Lodahl, S. Longo, A. Crosato and H. Wallace (1994). Intra-wave sediment transport in an oscillatory flow superimposed on a mean current, Delft Hydraulics Data report, H 1684, Part III, August.
- Katopodi, I., J.S. Ribberink, P. Ruol and C. Lodahl (1994a). Sediment transport measurements in combined wave current flows, Proc. Coastal Dynamics '94, Barcelona, Spain, ASCE, pp. 837-851.
- Ramadan, K.A.H. (1994). Time-averaged sediment transport phenomena in combined wave-current flows, M.Sc. Thesis, IHE Delft, Delft Hydraulics Report H1889.11, Part I, January.
- Ribberink, J.S. (1994). Time-averaged sediment transport phenomena in combined wave-current flows, Delft Hydraulics, Data-Report H1889.11, Part II, December.
- Ribberink, J.S. and A.A. Al-Salem (1994). Sediment transport in oscillatory boundary layers in cases of rippled beds and sheet flow, J. of Geoph. Res., Vol. 99, No. C6, pp. 12707-12727, June 15.